Biosensors and Bioelectronics 222 (2023) 115006

Contents lists available at ScienceDirect

Biosensors and Bioelectronics

journal homepage: www.elsevier.com/locate/bios

Attomolar detection of hepatitis C virus core protein powered by molecular antenna-like effect in a graphene field-effect aptasensor

Irene Palacio [a,*], Miguel Moreno [b], Almudena Náñez [b], Agnes Purwidyantri [c], Telma Domingues [c,d], Patrícia D. Cabral [c,d], Jérôme Borme [c], Marzia Marciello [e], Jesús Ignacio Mendieta-Moreno [f], Beatriz Torres-Vázquez [b,g], José Ignacio Martínez [a], María Francisca López [a], Mar García-Hernández [a], Luis Vázquez [a], Pavel Jelínek [f], Pedro Alpuim [c,d,**], Carlos Briones [b,h,***], José Ángel Martín-Gago [a,****]

[a] Institute of Material Science of Madrid (ICMM-CSIC), C/Sor Juana Inés de La Cruz 3, 28049, Madrid, Spain
[b] Centro de Astrobiología (CAB, INTA-CSIC), 28850, Torrejón de Ardoz, Madrid, Spain
[c] International Iberian Nanotechnology Laboratory (INL), 4715-330, Braga, Portugal
[d] Centro de Física das Universidades do Minho e Porto (CF-UM-UP), Universidade do Minho, 4710-057, Braga, Portugal
[e] Department of Chemistry in Pharmaceutical Sciences, Faculty of Pharmacy, Complutense University (UCM), Plaza Ramón y Cajal, 28040, Madrid, Spain
[f] Institute of Physics, Czech Academy of Sciences, 16200, Prague, Czech Republic
[g] Universidad de Alcalá, Facultad de Medicina, Madrid, Spain
[h] Centro de Investigación Biomédica en Red de Enfermedades Hepáticas y digestivas (CIBERehd), Instituto de Salud Carlos III, Madrid, Spain

ARTICLE INFO

Keywords:
Graphene
FET-biosensors
Aptamers
Covalent functionalization
HCV

ABSTRACT

Biosensors based on graphene field-effect transistors have become a promising tool for detecting a broad range of analytes. However, their performance is substantially affected by the functionalization protocol. In this work, we use a controlled in-vacuum physical method for the covalent functionalization of graphene to construct ultra-sensitive aptamer-based biosensors (aptasensors) able to detect hepatitis C virus core protein. These devices are highly specific and robust, achieving attomolar detection of the viral protein in human blood plasma. Such an improved sensitivity is rationalized by theoretical calculations showing that induced polarization at the graphene interface, caused by the proximity of covalently bound molecular probe, modulates the charge balance at the graphene/aptamer interface. This charge balance causes a net shift of the Dirac cone providing enhanced sensitivity for the attomolar detection of the target proteins. Such an unexpected effect paves the way for using this kind of graphene-based functionalized platforms for ultrasensitive and real-time diagnostics of different diseases.

1. Introduction

In recent years, the need for highly sensitive, fast, label-free, portable, and low-cost biosensing platforms has motivated extensive research and different transduction strategies (Balderston et al., 2021; Gao et al., 2016; Kim et al., 2019; Mani et al., 2009; Senior, 2014; Wang, 2008; Zheng et al., 2005). Among them, solution-gated field-effect transistors (SGFETs) have become a current trend (Ang et al., 2008; Campos et al., 2019; Hess et al., 2011; Seo et al., 2020) as they allow for sensitive and label-free identification of different analytes, such as proteins (including enzymes, antibodies, and structural proteins) or nucleic acids (Dong et al., 2010; Huang et al., 2010; Mao et al., 2010). This biosensing system is based on chemical conformation changes of the probe-target pair upon molecular recognition, which are transduced into an electrical signal. Recently, graphene's outstanding electrical properties and chemical inertness made it a valuable transduction

* Corresponding author.
** Corresponding author. International Iberian Nanotechnology Laboratory (INL), 4715-330, Braga, Portugal.
*** Corresponding author. Centro de Astrobiología (CAB, INTA-CSIC), 28850, Torrejón de Ardoz, Madrid, Spain.
**** Corresponding author.
E-mail addresses: i.palacio@csic.es (I. Palacio), pedro.alpuim.us@inl.int (P. Alpuim), cbriones@cab.inta-csic.es (C. Briones), gago@icmm.csic.es (J.Á. Martín-Gago).

https://doi.org/10.1016/j.bios.2022.115006
Received 12 September 2022; Received in revised form 23 November 2022; Accepted 9 December 2022
Available online 10 December 2022

platform for these devices (Dai et al., 2021; Heller et al., 2010; Kostarelos and Novoselov, 2014; Wang et al., 2016; Wang and Jia, 2018), resulting in an improved limit of detection (LoD) and biocompatibility (Béraud et al., 2021; Dai et al., 2021). However, the poor stability on the surface of the immobilized probe biomolecule leads to graphene-SGFET (g-SGFET) biosensors lacking the reproducibility and robustness required for stepping into the market (Holzinger et al., 2014).

The fabrication of g-SGFET platforms requires graphene functionalization, which is a difficult process due to the inherent chemical inertness of this nanomaterial. Non-covalent functionalization (Huang et al., 2010; Saltzgaber et al., 2013) has been presented as a better alternative for the construction of g-FET-based biosensors, arguing that covalent chemical functionalization jeopardizes the aromatic lattice of the graphene network and thus its electrical performance (Zhang et al., 2020). Here, we use a highly controlled covalent functionalization strategy based on ion-sputtering in ultra-high vacuum (UHV) and p-aminothiophenol (pATP) linker molecules that preserves graphene properties and allows precise control of the density of immobilized probe molecules (Bueno et al., 2017), differently of what is usually found in the literature (Fig. 1a). We report a g-SGFET aptasensor with improved reliability, specificity, and attomolar sensitivity to detect the hepatitis C virus (HCV) core protein, whose molecular probe is a chemically modified version of an *in vitro* evolved, high-affinity DNA aptamer (Torres-Vázquez et al., 2022). *In vitro* selected nucleic acid aptamers have shown several advantages over antibodies as molecular probes for developing biosensors with higher sensitivity, reproducibility, and robustness (Kaur et al., 2018; Liu et al., 2021). In recent years, high-affinity aptamers that detect relevant molecular targets, including proteins and nucleic acids from pathogenic viruses, have been obtained (Kim and Lee, 2021; Zou et al., 2019). HCV is a relevant human pathogen, the primary etiological agent of chronic hepatitis C (Manns et al., 2017; Pietschmann and Brown, 2019). It is estimated that around 58 million people have chronic hepatitis C worldwide, and up to 1.5 million new HCV infections occur yearly (WHO, 2021).

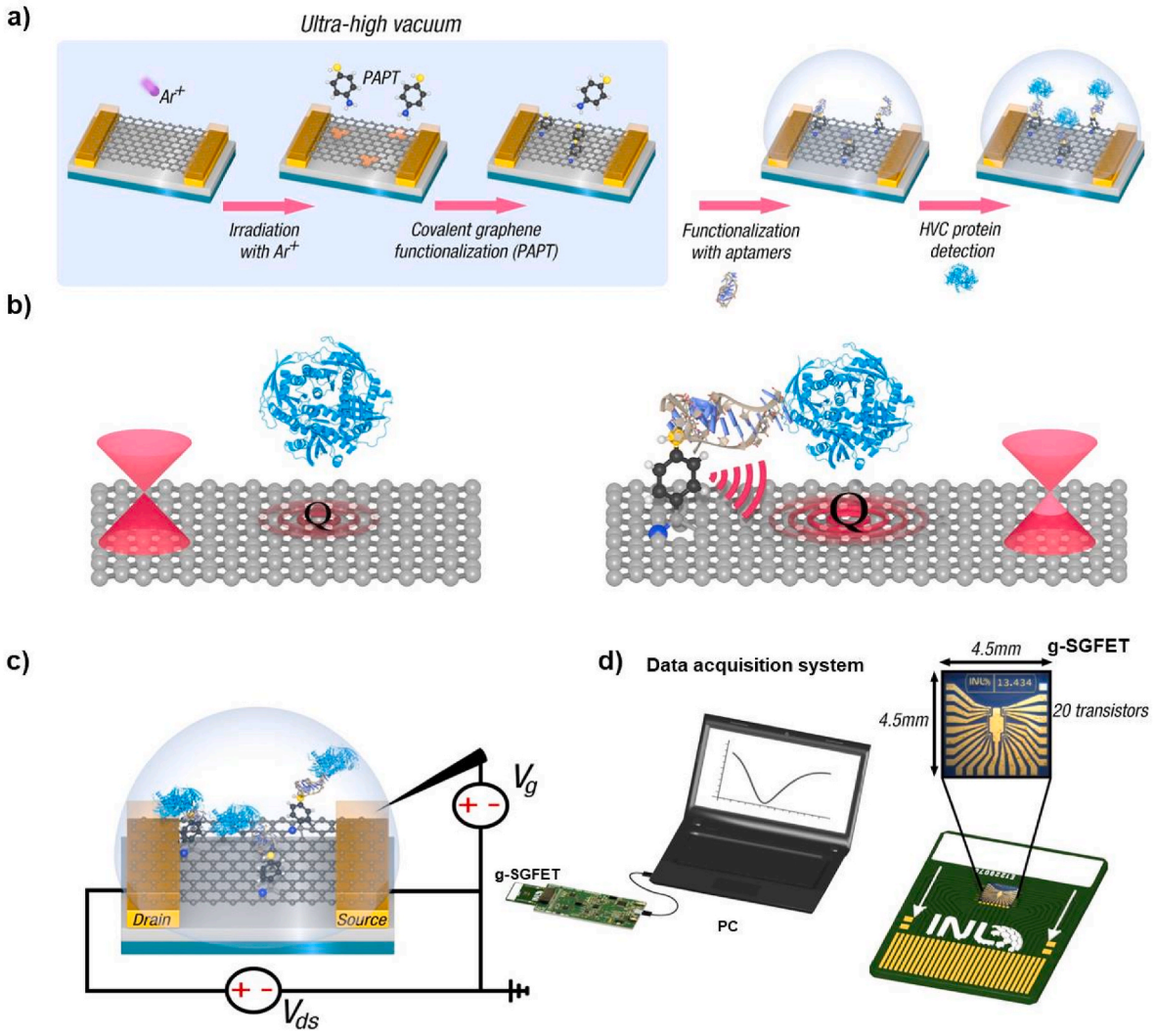

Fig. 1. a) Protocol to develop a covalent g-SGFET aptasensor. The first steps, carried out in UHV, consist of the covalent functionalization of the g-SGFET through a highly controlled methodology, after which a functional platform is obtained. This robust platform is functionalized with our previously selected aptamer that shows high specificity and affinity against HCV core protein. These two final steps are not carried out in UHV but in a liquid environment. b) Molecular-antenna effect: the covalently bound pATP linker acts as a molecular antenna enhancing the local polarization of graphene due to the proximity of the aptamer/protein system, setting the position of the Dirac cone. c) g-SGFET functioning scheme. The g-SGFET contains three terminals: the source, drain, and gate electrodes, and the active channel formed by a semi-metallic material, graphene, in this scenario. The charge carriers (electrons or holes) flow through the active channel from the source to the drain. The gate modulates the channel conductivity by applying a gate voltage that moves the graphene Fermi energy up or down in the density of states (DOS) for positive or negative voltages. d) Real image and dimensions of the g-SGFET wire-bonded to a printed circuit board (PCB) inserted into an electronic platform that can communicate with a computer where the measured data are displayed.

The remarkable performance of our device is understood in light of theoretical calculations showing that the covalently bound pATP linker is susceptible to the local polarization of graphene due to the proximity of the aptamer/protein system. The unprecedented sensitivity of the HCV core protein sensor is due to the linear energy-momentum band dispersion with vanishing density of the states at the Dirac point. This characteristic reduced electron density of states at the Dirac cone results in a high sensitivity to a charge transfer at the graphene/molecule interface, measured as a Dirac point shift providing the base for the sensing mechanism. From this perspective, the pATP linker can be considered a molecular antenna, which can capture a subtle charge transfer at the linker/graphene interface driven by the local polarization of graphene by the proximity of the aptamer/protein system (Fig. 1b).

The global COVID-19 pandemic has made it evident that advanced and ultrasensitive biosensors are required for early diagnosis of viral infections and, consequently, to monitor and reduce the spread of many infectious diseases. Our highly-controlled strategy to functionalize graphene platforms and the theoretical description of the complex mechanism underlying its improved performance pave the way for extended use of g-SGFET covalent biosensors with an expected growing number of clinical applications. This technology is easily scalable in an inexpensive configuration and transportable to the point of care (PoC) in clinical environments. Additionally, we anticipate that the molecular antenna effect described here can be generalized to other graphene-based devices.

2. Materials and methods

2.1. g-SGFET fabrication

A 200 mm silicon (Si) wafer (p-type doped with boron) with 100 nm of thermal oxide was used as substrate (Siegert Wafer, 8P0/1-100/725 ± 50/SSP/100 nm SiO_2). The wafer was sputter-coated with chromium (Cr, 3 nm) as an adhesion layer, gold (Au, 35 nm) as the conductive layer, and an alumina (Al_2O_3, 20 nm) capping. The source, drain, and gate electrodes were patterned by optical lithography and ion milling. A sacrificial layer (TiWN, 5 nm; AlSiCu, 100 nm; TiWN, 15 nm) was sputtered and patterned by lift-off to protect the entire wafer except for the islands where graphene will sit. After the dissolution of the Cu (Cu foil, 99.99 + % purity, Good Fellow, CU000410) catalyst in $FeCl_3$, HCl, and deionized water cycles, CVD-grown graphene supported by polymethylmethacrylate (PMMA) temporary substrate was wet transferred onto the wafer surface. Graphene was then patterned using optical lithography and oxygen plasma etching, and the sacrificial layer was removed by wet etch. A protective layer (Ni, 10 nm; AlSiCu 30 nm; TiWN 10 nm) was sputtered and patterned by lift-off to work as a stopping layer for the reactive ion etching of the multi-stack SiO_2 and SiN_x. The SiO_2 and SiN_x multi-stack passivation system (total thickness of 250 nm) was then deposited by plasma-enhanced CVD, patterned by optical lithography, and etched to cover the entire sensor area except for the graphene channel and contact pads. The wafer was then diced and cleaned with acetone, propanol, and deionized water. The chips were glued onto a homemade PCB, wire-bonded with gold wires, and protected with silicone elastomer. The solvents used during this process were: Dimethylformamide (DMF) (99.75% purity, Sigma-Aldrich, 484016), Ethanol (99.8%, Honeywell, 603-002-00-5) in addition to Ethanolamine, 98% (ETA), Sigma-Aldrich, E9508).

2.2. g-SGFET covalent functionalization

The functionalization protocol of g-SGFET takes place in a UHV chamber (base pressure 2 x 10^{-10} mbar). The protocol is a two-step process: i) the creation of single-atom vacancies in the graphene layer of the transistor with an Ar^+ ion sputter gun (E = 0.14 KeV); ii) the evaporation of 27 Langmuir of pATP (Sigma Aldrich, 97%). For further details, see (Bueno et al., 2017). We have confirmed that the functionalized graphene platforms are stable for at least several months.

2.3. Aptamer synthesis and incubation in the g-SGFET

Recently, single stranded (ss) DNA and RNA aptamers have been selected *in vitro* against six variants of HCV core protein, a highly conserved and multifunctional molecule that forms the viral capsid and performs additional, relevant functions in the HCV life cycle. Among them, the 76 nt-long ssDNA aptamer termed AptD-1312 (with nucleotide sequence 5′- GCGGATCCAGACTGGTGTGCCGTATCCCT CCCTTGTAATTATTTGTTCCATCCGTTCCGCCCTAAAGACAAGCTTC-3′) was highly represented in the final population of all the *in vitro* selection processes performed. It showed high affinity and specificity for the six HCV core variants used as selection targets (with a dissociation constant, *Kd*, value as low as 0.5 nM for the target termed G1-122, corresponding to the 122 amino acids long, hydrophilic domain of HCV core of genotype 1), and was shown to inhibit the HCV capsid assembly and viral replication in cell culture (Torres-Vázquez et al., 2022). Therefore, this aptamer was used as an optimal probe molecule for the detection of HCV core protein in g-SGFET-based aptasensors. With that aim, a thiol-derivatized version of AptD-1312 was synthesized, which contained a thiohexyl motif [HS–$(CH_2)_6$–] at its 5′ end (IBA-Life sciences, Göttingen, Germany). In parallel, a synthetic, 76 nt-long and thiohexyl-modified ssDNA molecule termed D-ACTG, which contains 10 repeats of the tetranucleotide ACTG in its central region [sequence 5' -GCGGATCCAGACTGGTGT$(ACTG)_{10}$GCCC-TAAAGACAAGCTTC-3'], was purchased to the same provider and immobilized onto biosensor surfaces as a negative control.

The immobilization of thiol-modified molecules AptD-1312 or D-ACTG onto transistor surface was performed following a procedure based on a previously described protocol (Bueno et al., 2017). Briefly, a 100 nM solution of each thiolated ssDNA (in a reaction buffer, RB, composed of 100 mM NaCl, 1 mM $MgCl_2$ and 100 mM HEPES pH 7.4) was folded into its reactive 3D structure by denaturation at 95 °C for 10 min, and then incubation at 25 °C for 10 min. Then, 10 μL of the renatured, thiolated ssDNA were deposited onto the ATP-modified graphene surface and left to react via disulfide bridge in a humidity chamber at 25 °C for 30 min. Afterwards, the ssDNA-modified surface was washed three times using RB. Finally, 10 μL of RB were deposited onto the transistor surface and the basal signal was measured.

2.4. HCV core protein detection and specificity tests

The AptD-1312-based aptasensor was subsequently incubated with 10 μL of HCV core protein (variant G1-122, expressed in baculovirus-insect systems by Algenex, Madrid, Spain; see (Torres-Vázquez et al., 2022)) ranging from 10^{-11} M to 10^{-18} M at 10-fold decreasing concentrations, either in RB or in human blood plasma of a HCV-negative donor (verified by antigenic tests and PCR) who provided a written consent that allowed the authors to use this plasma sample for diagnostic purposes (no further approval was required). The accuracy of the dilutions was checked by spectrophotometry, using a Nanodrop 1000 spectrophotometer (Thermo Scientific, Madison, Wisconsin, USA).The target protein was incubated in a humidity chamber for 20 min at 25 °C. Then, the biosensor surface was washed three times using RB to discard the protein molecules that could remain non-specifically bound to the surface. 10 μL of RB were deposited onto the transistor surface and the signal (the aptamer-protein bio-identification process, which is converted into an electrical response) was measured.

A control experiment was performed using a D-ACTG-modified biosensor under the experimental conditions described above. Additionally, the specificity of the AptD-1312 aptasensor was evaluated by exposing it to the protein bovine serum albumin (BSA; Sigma, Saint Louis, Missouri, USA) under the same experimental conditions described above, at a concentration of 10^{-14} M in RB. Finally, to evaluate the specificity of AptD-1312 for the detection of HCV core in a relevant

biological fluid, the biosensor was exposed to human plasma of a verified HCV negative individual, which contains many proteins and other potentially interfering biomolecules. The aptasensor was then incubated with 10 μL of HCV core protein ranging from 10^{-11} M to 10^{-18} M at 10-fold decreasing concentrations in such a HCV-negative human plasma.

2.5. g-SGFET electrical characterization

For the Dirac point extraction from the g-SGFET transfer curves, the PCB carrying the g-FET chip was plugged in a built-in credit-card-size Arduino-like board consisting of a microcontroller, a 16-bit digital-to-analog converter (DAC, nº pLTC2602; and ADC from Texas Instrument, ref. ADS8685), an 8-bit digital potentiometer, a resistance-controlled current source of 1–100 μA, and complementary metal-oxide-semiconductor (CMOS) matrices. The setup was connected to a desktop computer to monitor the sensor arrays' output signal from up to twenty transistors by setting the measurement parameters from a graphical user interface. A 1 mV voltage was applied between the source and drain (V_{DS}). The gate was swept from 0.3 to 0.7 V with a voltage step of 10 mV. A single measurement consists in using the 20 sensors successively, with 1 s waiting time between each measurement of the transfer curve.

2.6. Theoretical modelling

For the simulations, the structure has been relaxed using QM/MM scheme with Fireball/Amber (Mendieta-Moreno et al., 2014) where the graphene and linker are in the QM region and the aptamer and the complementary bases in the MM region. The PDOS was calculated with the whole system in Density Functional Theory (DFT) using Fireball (Lewis et al., 2011), and the partial charge also with Fireball DFT was calculated with Löwdin charges (Löwdin, 1950). All the simulations with Fireball have been done with a minimal basis with s orbital for H, sp^3 orbitals for C, N, O, Na and S, and sp^3d^5 orbitals for P.

3. Results and discussion

3.1. Ultra-sensitive aptasensor

The functionalization and testing process of the g-SGFET aptasensor developed in this work is schematized in Fig. 1. The first step is fabricating the device, consisting of a sensor array of 20 graphene channels with a shared gate contact and an individually addressable channel, using clean-room technology (Cabral et al., 2020) (see Materials and methods). The golden gate electrode is covered by a self-assembled monolayer (SAM) of dodecanethiol (DDT), following the protocol indicated in ref. (Fernandes et al., 2019) (see Supplementary data). Once the chip is fabricated, it is placed in an UHV chamber for the physical covalent functionalization of graphene, using a two-step protocol recently developed (Bueno et al., 2017, 2019) (Fig. 1a). This methodology preserves graphene's electronic properties associated with its atomic structure while ensuring atomically precise control and cleanliness. In the first step, single-atom vacancies are formed in the graphene layer by low-energy Ar^+ ions. As a result, the inert graphene turns into a highly reactive surface due to the generated dangling bonds at carbon vacancies. At this moment, pATP linker molecules are evaporated in the UHV chamber by physical vapor deposition (PVD). The linker gets covalently coupled to the surface, its N atom anneals the vacancy, and the thiophenol motif adopts an upright configuration onto one of the neighbouring C atoms, exposing thiol-free groups towards the vacuum as explained below. This structural geometry is essential for the performance of the device: first, it will keep the aptamer (and, then, the aptamer/protein complex) at a short distance of the surface, and second, it will play the role of a molecular antenna that will locally induce polarization on the graphene in such a way that the g-SGFET will record a change in channel conductance.

Once all the induced graphene surface vacancies are covered with the linker, the g-SGFET is removed from UHV. We checked by a colorimetric method (details in the Supplementary data, Fig. S3) that the functionalized g-SGFET maintains its free thiol groups in a reduced and reactive state for months. Subsequently, a 10 μL drop of the renatured, thiol-modified ss DNA aptamer AptD-1312 in a buffer solution (see Materials and methods) is placed onto the sensor and left to react in a humidity chamber for 30 min at 25 °C (Fig. 1a). The aptamer binds the linker via covalent disulfide bonds, and thus the functionalized platform becomes an aptasensor for the biorecognition of HCV core protein. Each sequential adsorption step was followed by atomic force microscopy (AFM) images (see Supplementary data, Fig. S4). Analysis of the surface shows that the graphene surface is not damaged by the chemistry performed along the steps indicated in Fig. 1a.

3.2. Attomolar detection of HCV core protein

Fig. 2a shows graphene's charge neutrality point movement detected as the gate voltage (V_{Dirac}) corresponding to the minimum I_{DS} current in the transistor transfer curves acquired after successive functionalization stages before biorecognition. The first V_{Dirac} point (bare graphene) indicates unintentional slightly p-doping due to the exposure to atmospheric conditions and hence to the p-doping effect of oxygen (Zhang et al., 2011). Subsequent steps consistently shift the charge neutrality point towards zero gate voltage: first, after the DDT treatment, and second, after covalent functionalization with the pATP linker molecule. When the g-SGFET is functionalized with the aptamer, V_{Dirac} slightly shifts in the opposite direction, indicating p-doping. Two chips (chip 1 and chip 2) are prepared for subsequent incubation of target protein molecules in the buffer and human plasma. Trends are similar in both chips (Fig. 2a), indicating good reproducibility of the graphene surface functionalization procedure. Further reproducibility experiments can be found in the Supplementary data (Fig. S5).

For the analytic detection of the HCV core protein, the g-SGFET aptasensor was exposed to either a buffer or a human blood plasma, which were in both cases supplemented with HCV core protein at different concentrations (see Materials and methods). Fig. 2b and c shows the characteristic transfer curves (TCs) obtained after HCV virus core protein incubation in buffer and plasma at concentrations from 10^{-18} to 10^{-11} M. In both cases, consecutive V_{Dirac} negative shifts result for every 10-fold increase of the core protein concentration, as shown in Fig. 2d and e, which plot the V_{Dirac} as a function of the HCV core protein concentration. This shift indicates an effective graphene n-doping. The calibration curve in the buffer (Fig. 2d) shows a linear device response for protein concentrations over four decades, from 10^{-14} to 10^{-18} M, with a 14 mV/decade sensitivity. The saturation point in the buffer occurs at 10 fM. The LoD is 15.6 aM (see details on how it is calculated in the Supplementary data). The size of relative standard deviation (RSD) bars results from the statistical analysis of all the transfer curves (10) generated by recording simultaneously up to 20 transistors per chip. Details on the RDS, fitting lines, and dose-response fittings in Fig. 2d and e can be found in the Supplementary material.

We also exposed the biosensor to human blood plasma, containing a great variety of proteins and other biomolecules, from an HCV-negative donor, supplemented with HCV core protein at concentrations between 10^{-18} and 10^{-11} M. Fig. 2e shows the linear device response for HCV core protein concentrations spanning five decades, from 10^{-13} to 10^{-18} M. A sensitivity of 15 mV/decade and a saturation point at 100 fM are found with the corresponding LoD at 90.9 aM. The result of this experiment is similar to that obtained with HCV core protein in a buffer solution, which shows that our aptasensor allows the detection of HCV core protein in human plasma with high sensitivity (attomolar level) and specificity (without observing side effects potentially due to the proteins or other biomolecules contained in the plasma). Therefore, the g-SGFET-based aptasensor developed here meets the requirements for testing in the clinical setting as a diagnostic tool for HCV in infected patients. The

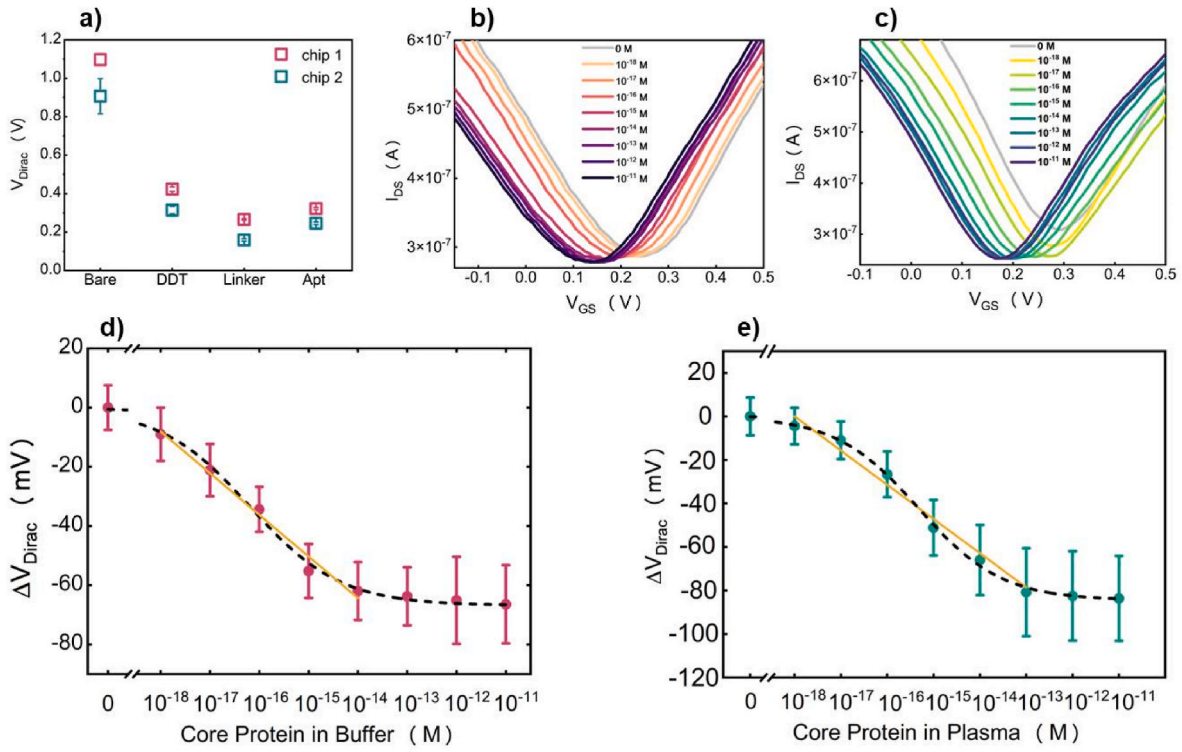

Fig. 2. Electrical response of the g-SGFET aptasensor device. a) g-SGFET V_{Dirac} point initial position after each functionalization stage before HCV core protein detection: bare graphene, DDT treatment, covalent functionalization with the pATP linker, and aptamer functionalization, in two different chips (chip 1 and 2). b) and c) Characteristic transfer curves in a buffer solution (b) and human blood plasma (c) for the HCV core protein concentrations studied (10^{-18} to 10^{-11} M). d) and e) Effective response extracted from the I_{DS} current generated by the different HCV protein concentrations and fitted to a dose-response (dashed line) for buffer (d) and human plasma (e) solutions (the R^2 of the fitting lines are 0.98 and 0.96 in buffer and plasma, respectively).

high reproducibility of the results has been demonstrated by measuring in different aptasensors, as shown in the Supplementary data (Figs. S6 and S7).

The specificity of the aptasensor to HCV core protein has been further studied by its response to another protein which is unspecific for the aptamer probe, bovine serum albumin (BSA), at a representative concentration of 10^{-14} M (see Materials and methods) (Fig. 3a and b). The measured V_{Dirac} did not show a significant variation in the presence of

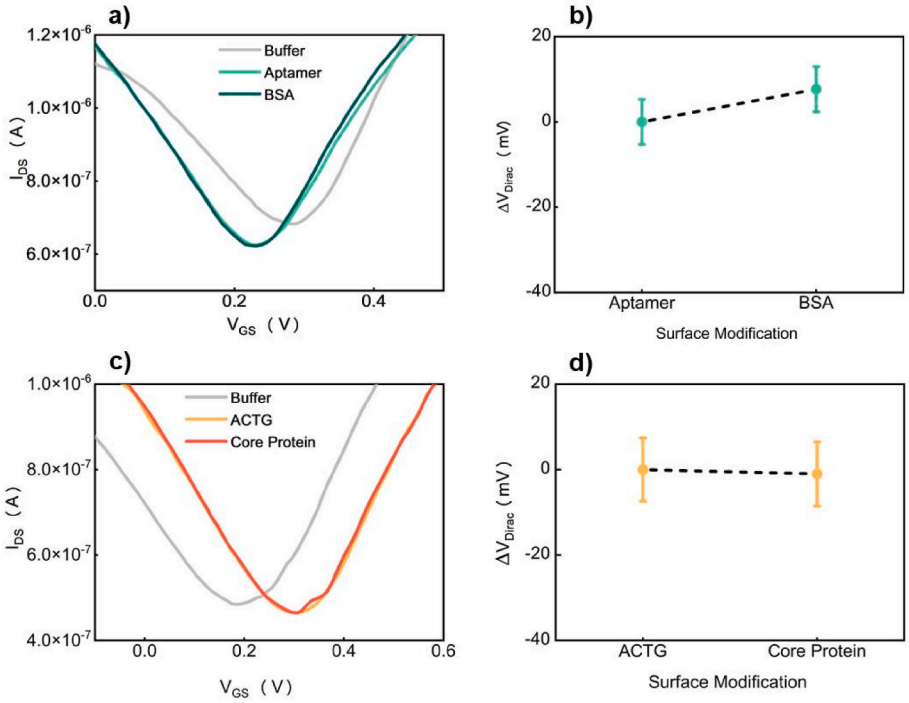

Fig. 3. Specificity tests of the g-SGFET aptasensor. **a)** Transfer curves and **b)** V_{Dirac} variation showing the biosensor's lack of response to an unspecific protein (BSA). **c)** Transfer curves and **d)** V_{Dirac} variation showing the biosensor's lack of response for HCV core protein when the unspecific DNA sequence D-ACTG (see Materials and methods) had been covalently immobilized onto the graphene surface instead of the AptD-1312 aptamer. The sensor exhibits almost zero response in both cases (i.e., almost zero V_{Dirac} shift), thus showing adequate specificity.

BSA. Another control experiment was performed by functionalizing the graphene surface with the ssDNA molecule D-ACTG (see Materials and methods). As expected, the measured V_{Dirac} showed no differences before and after exposition against the HCV core protein (Fig. 3c and d). Further specificity tests can be found in the Supplementary data (Figs. S8 and S9).

3.3. The molecular antenna amplification effect

To gain more insight into the understanding of the covalent functionalization of graphene and the operating mechanism of the aptasensor, we carried out DFT and quantum mechanics/molecular mechanics (QM/MM) simulations (see Materials and methods) to monitor how different covalently linked functional groups affect the position of the Dirac cone relative to the Fermi level, i.e., the V_{Dirac} shift.

According to the total energy DFT calculations, incorporating pATP via its amine group into a single C atom vacancy of the bare graphene is energetically unstable. Namely, we found a configuration consisting of a nitrogen atom filling the vacancy and a covalently linked thiophenol group bound to a carbon atom next to the substitutional nitrogen (see Fig. 4a and Fig. S10), which is more stable (by ~ 1.8 eV) than the direct incorporation of an amine group into the vacancy. Moreover, the free activation energy for the shift of the thiophenol group from the N-defect to an adjacent carbon atom is almost negligible (dE = 0.14 eV). Based on these findings, we propose the following scenario: the direct incorporation of the amine group into the graphene vacancy is accompanied by an amine dehydrogenation process that destabilizes the covalent C–N bond on the phenyl group; this instability causes breakage of the C–N bond accompanied by the shift of the thiophenol onto the adjacent carbon atom, adopting an energetically more stable configuration (Fig. 4a).

The calculation of the following stages towards the biorecognition cannot be performed with the whole aptamer/protein system because the HCV core protein structure is unknown, and the number of atoms involved in the interaction with the aptamer is very high. Thus, we used a simple model that mimics the primary underlying physical process occurring in the proximity of the sensor surface. An aptamer interacts with its target protein through H-bonds (and other non-complementary interactions) established between the DNA backbone and nucleobases of the first and the amino acids of the later. It is striking that the mere presence of H-bonds induces a significant shift of the V_{Dirac}, as charge cannot flow to (from) the graphene surface. To simulate this process, we have simplified the system to the minimum configuration that retains most of the physical features. Thus, we model the aptamer by its first three DNA nucleotides bound to the graphene layer through a pATP molecule. The presence of the target protein, to which the aptamer specifically binds through non-covalent bonds, is simulated by single DNA nucleobases that interact with the complementary nucleobases of

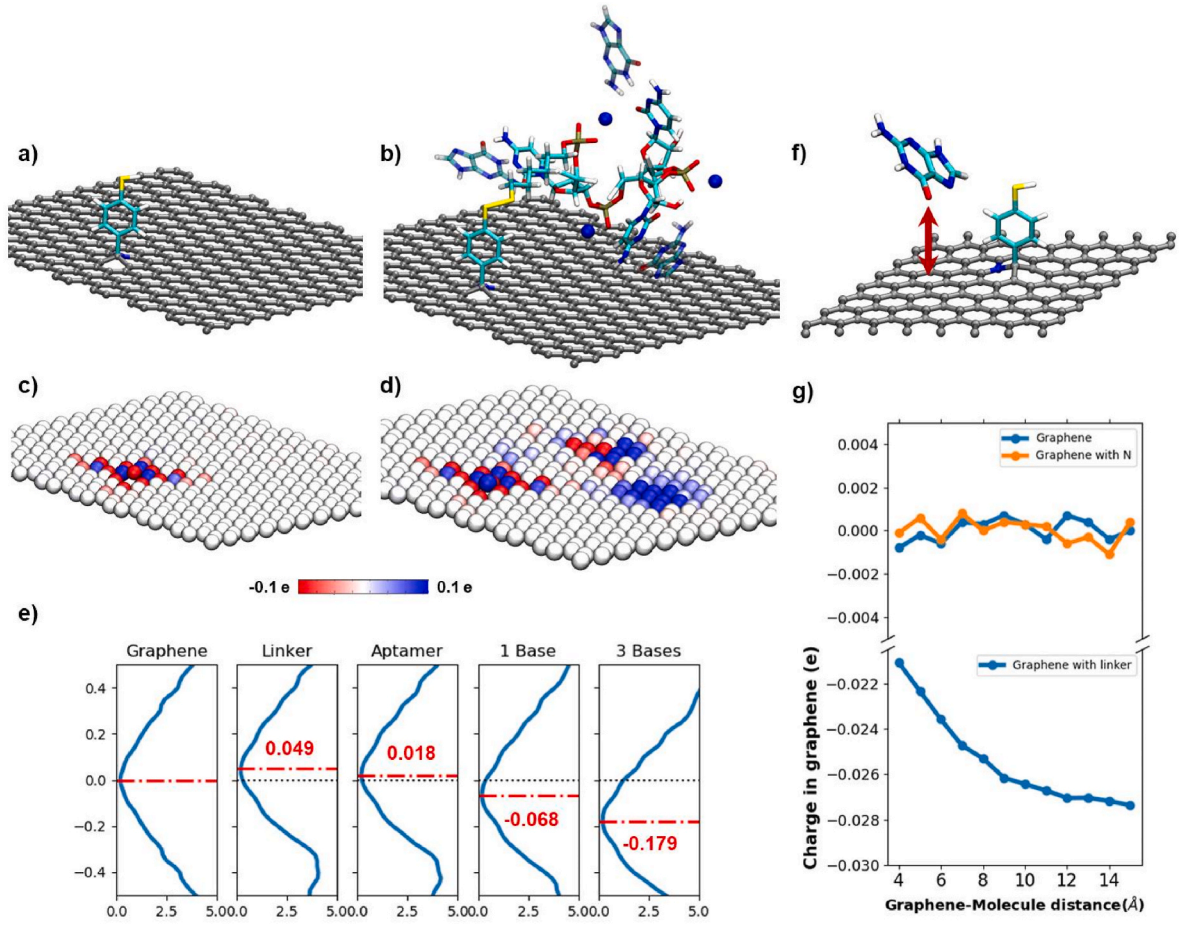

Fig. 4. Protein detection mechanism. a) Adsorption geometry for the pATP linker molecule covalently bound to graphene. **b**) Adsorption geometry of the linker plus the aptamer modeled by its first three DNA nucleotides in the presence of the target protein mimicked by single DNA nucleobases in an ionic solution. **c**) and **d)** Plots of the partial atomic charges in the graphene sheet when the linker (c) is covalently bound and when the aptamer and the viral protein (d) are also bound in the graphene surface (red color/negative value represents the excess of atomic charge, while blue color/positive value means loss of atomic charge). **e**) Variation of the PDOS of the different states over the functionalization and biodetection. The Fermi level is aligned to zero energy to ease the direct comparison of the V_{Dirac} shift. **f)** Structure of the graphene with the pATP linker and a guanine nucleobase. The arrow indicates the variation in height distance with graphene. **g)** Variation of the summed charge in the graphene sheet at different heights of the guanine.

the aptamer through H-bonds in a liquid environment (Fig. 4b). Although it may seem surprising to consider nucleobases instead of amino acids to mimic the aptamer-protein complex, we have preferred to use those as the interaction of the aptamer with the amino acids from the protein is mainly established through H-bonds, whose direction is dictated by the structure of the complex. As this structure is unknown in our case, the sole and simple way of simulating a stable H-bond interaction is by using the complementary nucleobase in the calculation. Thus, we have considered cytosine in the aptamer structure and a free guanine to mimic at first approximation, the interaction of the aptamer with an amino acid of the core protein.

Fig. 4e shows the variation of the projected density of states (PDOS) in the graphene channel along the different steps of the functionalization and detection process, namely the addition to the pristine graphene of i) pATP linker, ii) aptamer, iii) aptamer with one complementary nucleobase interacting through H-bonding, iv) aptamer with three complementary nucleobases bound relative to the pristine graphene. The Fermi level is aligned to zero energy to ease the direct comparison of the V_{Dirac} shift. According to the DFT simulations, the covalent functionalization of graphene by thiophenol and the incorporation of the substitutional nitrogen atom leads to charge transfer to the graphene, causing a slight shift of the Dirac cone above the Fermi level (Fig. 4e). Interestingly, this shift is opposite to that expected for a substitutional N-doping in graphene. In this case, there is charge transfer from the N-defect to the neighbor carbon atoms (Mallada et al., 2020; Telychko et al., 2014), causing a shift of the Dirac cone below the Fermi level. The covalently linked thiophenol to a carbon atom adjacent to the substitutional N-defect overcomes this n-doping effect pushing the Dirac cone slightly above the Fermi level. Thus, the covalent bonding of the linker (thiophenol) and the presence of the substitutional nitrogen atom cause the direct charge transfer from the graphene sheet via the covalent bonding. The effect is also demonstrated by the intense polarization of graphene atoms near the covalent bond (Fig. 4c and Figs. S11 and S12 of the supplementary data). Interestingly, this local polarization of atomic charges surrounding the covalently bonded linker remains at first glance almost intact after further functionalization of the graphene (Fig. 4d, Figs. S11 and S12). On the other hand, we found that the shift of V_{Dirac} correlates nicely with the total accumulated atomic charge in the graphene (Fig. S12). The proximity of charged groups of the aptamer backbone (in particular, phosphate moieties) and nucleobases (amino groups) gives rise to local polarization of the graphene sheet (Fig. 4d), which modulates the position of the Dirac cone with respect to the Fermi level (Fig. 4e). Moreover, the simulations predict that adding more complementary nucleobases (as a proxy to the effect produced by the protein-ligand) leads to the further polarization of the graphene sheet underneath, causing additional downwards shift of $V_{Dirac.}$

To understand the detailed mechanism of this effect, we carried out simulations of a minimal system approaching a polar guanine nucleobase oriented by its ketone group towards either the pristine graphene or the covalently functionalized graphene with the thiophenol group (Fig. 4f). The accumulated atomic charge remains zero in the pristine graphene; consequently, the Dirac cone's position does not change. However, for pATP-functionalized graphene, the approximation of the polar guanine causes an accumulation of the charge in the graphene (Fig. 4g), which shifts the position of the Dirac cone below the Fermi level. Note that no changes are expected in the absence of covalent bonding, as experimentally confirmed in Fig. S9.

The local polarization of graphene by the proximity of the polar molecule disrupts the detailed charge balance between the graphene sheet and the pATP linker, causing the V_{Dirac} shift. Therefore, the linker behaves as a kind of molecular antenna, amplifying the local polarization in the graphene's vicinity. Notably, the characteristic vanishing density of states of graphene near the Dirac cone makes its position very sensitive to the local charge transfer. This effect provides an optimal mechanism for biosensing and underlines the advantages of using aptamers instead of antibodies (whose size and molecular weight are much larger) as molecular probes in graphene-based biosensors.

4. Conclusion

The covalent functionalization of thiophenol moieties on the graphene surface embodies a molecular antenna effect, which enhances the local polarization of graphene when the charged atoms from a polarized molecule are placed in its vicinity. We have used this effect to fabricate robust g-SGFET aptasensors showing attomolar sensitivity, reproducibility, and high specificity to detect HCV core protein in human blood plasma, which can thus be used for the early diagnosis of HCV infection. Covalently bound aptamers keeping the ligand at a fixed nanometric distance from the surface is the key to this sensing platform's enhanced features and broad applicability in different fields of research, including biotechnology and biomedicine.

CRediT authorship contribution statement

Irene Palacio: was in charge of the overall coordination of the work, designed the experiments and coordinated the work of the different teams, performed the FETs functionalization and the measurements with the FETs. **Miguel Moreno:** selected in vitro, synthesized and tested the aptamer. **Almudena Náñez:** selected in vitro, synthesized and tested the aptamer and performed the measurements with the FETs. **Agnes Purwidyantri:** performed the measurements with the FETs and the Raman spectroscopy. **Telma Domingues:** grew the graphene, fabricated the FETs, performed the Raman spectroscopy and the measurements with the FETs. **Patrícia D. Cabral:** grew the graphene, fabricated the FETs, performed the measurements with the FETs and the Raman spectroscopy. **Jérôme Borme:** grew the graphene, fabricated the FETs and performed the Raman spectroscopy. **Marzia Marciello:** performed the colorimetric thiol detection experiments. **Jesús Ignacio Mendieta-Moreno:** performed the DFT calculations. **Beatriz Torres-Vázquez:** selected in vitro, synthesized and tested the aptamer. **José Ignacio Martínez:** performed the DFT calculations. **María Francisca López:** supervised the functionalization protocols. **Mar García-Hernández:** supervised the functionalization protocols. **Luis Vázquez:** performed the AFM measurements. **Pavel Jelínek:** performed the DFT calculations. **Pedro Alpuim:** designed the experiments and coordinated the work of the different teams, grew the graphene and fabricated the FETs. **Carlos Briones:** designed the experiments and coordinated the work of the different teams, selected in vitro, synthesized and tested the aptamer. **José Ángel Martín-Gago:** conceived the general idea and was in charge of the overall coordination of the work. All authors contributed to the discussion and writing of the manuscript and have approved the submitted version.

Declaration of competing interest

The authors declare that they have no known competing financial interests or personal relationships that could have appeared to influence the work reported in this paper.

Data availability

Data will be made available on request.

Acknowledgments

This work has been supported by the EU Graphene Flagship funding (Grant Graphene Core3 881603), the Ministerio de Ciencia e Innovación of Spain: PID2020-113142RB-C21, the European Structural Funds via FotoArt-CM project (P2018/NMT-4367) and the Portuguese Foundation for Science and Technology (FCT) via the Strategic Funding UIDB/04650/2020. Work at CAB was funded by the Spanish Ministerio de Ciencia e Innovación (MICINN) grant no. PID2019-104903RB-I00 and

the Spanish Agencia Estatal de Investigación (AEI) Project no. MDM-2017-0737 - Unidad de Excelencia "María de Maeztu," and it also benefits from the interdisciplinary framework provided by CSIC through "LifeHUB.CSIC" initiative (PIE 202120E047-CONEXIONES-LIFE). CIBERehd is funded by Instituto de Salud Carlos III (ISCIII). A.N. is supported by the predoctoral fellowship PRE-CAB-BIOMOLECULAS 2 from INTA. B.T-V. is supported by the predoctoral fellowship TS17/16 from INTA and by the CSIC "Garantía Juvenil" contract CAM19_PRE_CAB_001 funded by Comunidad Autónoma de Madrid (CAM). FCT supports T.D. and P.C. under Ph.D. grants SFRH/BD/08181/2020 and SFRH/BD/128579/2017. M.M. would like to thank Comunidad de Madrid for the predoctoral grant IND2020/BIO-17523. P.A. and C.B. also acknowledge the support provided by La Caixa Foundation through Project LCF/PR/HR21/52410023. L. V. would like to thank Comunidad Autónoma de Madrid (TRANSNANOAVANSENS program: S2018-NMT-4349) and E.V. García-Frutos for her assistance during the AFM experiments.

Appendix A. Supplementary data

Supplementary data to this article can be found online at https://doi.org/10.1016/j.bios.2022.115006.

References

Ang, P.K., Chen, W., Wee, A.T.S., Kian, P.L., 2008. J. Am. Chem. Soc. 130, 14392–14393.
Balderston, S., Taulbee, J.J., Celaya, E., Fung, K., Jiao, A., Smith, K., Hajian, R., Gasiunas, G., Kutanovas, S., Kim, D., Parkinson, J., Dickerson, K., Ripoll, J.J., Peytavi, R., Lu, H.W., Barron, F., Goldsmith, B.R., Collins, P.G., Conboy, I.M., Siksnys, V., Aran, K., 2021. Nat. Biomed. Eng. 5, 713–725.
Béraud, A., Sauvage, M., Bazán, C.M., Tie, M., Bencherif, A., Bouilly, D., 2021. Analyst 146, 403.
Bueno, R., Marciello, M., Moreno, M., Sánchez-sánchez, C., José, I., Martinez, L., Prats-alfonso, E., Guimerà-brunet, A., Jose, A., Villa, R., Monpean, F., García-hernandez, M., Huttel, Y., 2019. ACS Omega 4, 3287–3297.
Bueno, R.A., Martínez, J.I., Luccas, R.F., Del Árbol, N.R., Munuera, C., Palacio, I., Palomares, F.J., Lauwaet, K., Thakur, S., Baranowski, J.M., Strupinski, W., López, M. F., Mompeán, F.J., García-Hernández, M., Martín-Gago, J.A., 2017. Nat. Commun. 8, 15306.
Cabral, P.D., Domingues, T., Machado, G., Chicharo, A., Cerqueira, F., Fernandes, E., Athayde, E., Alpuim, P., Borme, J., 2020. Materials 13, 5728.
Campos, R., Borme, J., Guerreiro, J.R., Machado, G., Cerqueira, M.F., Petrovykh, D.Y., Alpuim, P., 2019. ACS Sens. 4, 286–293.
Dai, C., Liu, Y., Wei, D., 2021. Chem. Rev. 122, 10319–10392.
Dong, X., Shi, Y., Huang, W., Chen, P., Li, L.-J., 2010. Adv. Mater. 22, 1649–1653.
Fernandes, E., Cabral, P.D., Campos, R., Machado, G., Cerqueira, M.F., Sousa, C., Freitas, P.P., Borme, J., Petrovykh, D.Y., Alpuim, P., 2019. Appl. Surf. Sci. 480, 709–716.
Gao, W., Emaminejad, S., Nyein, H.Y.Y., Challa, S., Chen, K., Peck, A., Fahad, H.M., Ota, H., Shiraki, H., Kiriya, D., Lien, D.H., Brooks, G.A., Davis, R.W., Javey, A., 2016. Nature 529, 509–514.
Heller, I., Chatoor, S., Männik, J., Zevenbergen, M.A.G., Dekker, C., Lemay, S.G., 2010. J. Am. Chem. Soc. 132, 17149–17156.
Hess, L.H., Jansen, M., Maybeck, V., Hauf, M.V., Seifert, M., Stutzmann, M., Sharp, I.D., Offenhäusser, A., Garrido, J.A., 2011. Adv. Mater. 23, 5045–5049.
Holzinger, M., Goff, A. Le, Cosnier, S., 2014. Front. Chem. 2, 63.
Huang, Y., Dong, X., Shi, Y., Li, C.M., Li, L.J., Chen, P., 2010. Nanoscale 2, 1485–1488.
Kaur, H., Bruno, J.G., Kumar, A., Sharma, T.K., 2018. Theranostics. 8, 4016–4032.
Kim, J., Campbell, A.S., de Ávila, B.E.F., Wang, J., 2019. Nat. Biotechnol. 37, 389–406.
Kim, T.-H., Lee, S.-W., 2021. Int. J. Mol. Sci. 22, 4168.
Kostarelos, K., Novoselov, K.S., 2014. Nat. Nanotechnol. 9, 744–745.
Lewis, J.P., Jelínek, P., Ortega, J., Demkov, A.A., Trabada, D.G., Haycock, B., Wang, Hao, Adams, G., Tomfohr, J.K., Abad, E., Wang, Hong, Drabold, D.A., 2011. Phys. Status Solidi 248, 1989–2007.
Liu, L.S., Wang, F., Ge, Y., Lo, P.K., 2021. ACS Appl. Mater. Interfaces. 13, 9329–9358.
Löwdin, P.O., 1950. J. Chem. Phys. 18, 365–375.
Mallada, B., Edalatmanesh, S., Lazar, P., Redondo, J., Gallardo, A., Zbořil, R., Jelínek, P., Švec, M., De La Torre, B., 2020. ACS Sustain. Chem. Eng. 8, 3437–3444.
Mani, V., Chikkaveeraiah, B.V., Patel, V., Gutkind, J.S., Rusling, J.F., 2009. ACS Nano 3, 585–594.
Manns, M.P., Buti, M., Gane, E., Pawlotsky, J.M., Razavi, H., Terrault, N., Younossi, Z., 2017. Nat. Rev. Dis. Prim. 3, 1–19.
Mao, S., Lu, G., Yu, K., Bo, Z., Chen, J., 2010. Adv. Mater. 22, 3521–3526.
Mendieta-Moreno, J.I., Walker, R.C., Lewis, J.P., Gómez-Puertas, P., Mendieta, J., Ortega, J., 2014. J. Chem. Theor. Comput. 10, 2185–2193.
Pietschmann, T., Brown, R.J.P., 2019. Trends Microbiol. 27, 379–380.
Saltzgaber, G., Wojcik, P.M., Sharf, T., Leyden, M.R., Wardini, J.L., Heist, C.A., Adenuga, A.A., Remcho, V.T., Minot, E.D., 2013. Nanotechnology 24, 355502.
Senior, M., 2014. Nat. Biotechnol. 32, 856.
Seo, G., Lee, G., Kim, M.J., Baek, S.H., Choi, M., Ku, K.B., Lee, C.S., Jun, S., Park, D., Kim, H.G., Kim, S.J., Lee, J.O., Kim, B.T., Park, E.C., Kim, S. Il, 2020. ACS Nano 14, 5135–5142.
Telychko, M., Mutombo, P., Ondráček, M., Hapala, P., Bocquet, F.C., Kolorenč, J., Vondráček, M., Jelínek, P., Švec, M., 2014. ACS Nano 8, 7318–7324.
Torres-Vázquez, B., María de Lucas, A., García-Crespo, C., Antonio García-Martín, J., Fragoso, A., Fernández-Algar, M., Perales, C., Domingo, E., Moreno, M., Briones, C., 2022. J. Mol. Biol. 434, 167501.
Wang, C., Cui, X., Li, Y., Li, H., Huang, L., Bi, J., Luo, J., Ma, L.Q., Zhou, W., Cao, Y., Wang, B., Miao, F., 2016. Sci. Rep. 6, 1–8.
Wang, J., 2008. Chem. Rev. 108, 814–825.
Wang, Z., Jia, Y., 2018. Carbon N. Y. 130, 758–767.
WHO, 2021. Global progress report on HIV; viral hepatitis and sexually transmitted infection. 2021 [WWW Document]. URL. https://www.who.int/publications/i/item/9789240027077.
Zhang, X., Jing, Q., Ao, S., Schneider, G.F., Kireev, D., Zhang, Z., Fu, W., 2020. Small 16, 1902820.
Zhang, Z., Huang, H., Yang, X., Zang, L., 2011. J. Phys. Chem. Lett. 2, 2897–2905.
Zheng, G., Patolsky, F., Cui, Y., Wang, W.U., Lieber, C.M., 2005. Nat. Biotechnol. 23, 1294–1301.
Zou, X., Wu, J., Gu, J., Shen, L., Mao, L., 2019. Front. Microbiol. 10, 1462.